DØNote 6166-CONF

Search for $ZH \to \ell^+\ell^- b\bar{b}$ production in 8.6 fb^{-1} of $p\bar{p}$ collisions

The DØ Collaboration
URL http://www-d0.fnal.gov

Dated July 20, 2011

We present a search for a standard model (SM) Higgs boson produced in association with a Z boson in 8.6 fb^{-1} of $p\bar{p}$ collisions, collected with the D0 detector at the Fermilab Tevatron at $\sqrt{s} =$ 1.96 TeV. Selected events contain one reconstructed $Z \to e^+e^-$ or $Z \to \mu^+\mu^-$ candidate and at least two jets, including at least one b-tagged jet. The data are consistent with the background expected from other SM processes. Upper limits at 95% C.L. on the ZH production cross section times branching ratio are set for Higgs boson masses $100 < M_H < 150$ GeV. The observed (expected) limit for $M_H = 115$ GeV is a factor of 4.9 (4.8) larger than the SM prediction.

Preliminary Results for Summer 2011 Conferences

I. INTRODUCTION

In the standard model (SM), the spontaneous breakdown of the electroweak gauge symmetry generates masses for the W and Z bosons and produces a residual massive particle, the Higgs boson, which has so far eluded detection. The discovery of the Higgs boson would be a remarkable addition to the list of experimentally confirmed SM predictions. For Higgs boson masses $M_H \lesssim 135$ GeV, the primary Higgs boson decay in the SM is to $b\bar{b}$, which has copious background at the Tevatron collider. Consequently, sensitivity to a low-mass Higgs boson is predominantly from its production in association with a W or Z boson.

We present a search for $ZH \to \ell^+\ell^- b\bar{b}$, where ℓ is either a muon or an electron. The search for $ZH \to \nu\bar{\nu}b\bar{b}$ is treated elsewhere [1]. The data for this analysis were collected at the Fermilab Tevatron Collider by the D0 detector [2] from April 2001 to February 2006 (Run IIa), and from June 2006 to March 2011 (Run IIb). Between Run IIa and Run IIb a new layer of the silicon microstrip tracker was installed, and the trigger system was upgraded. The analyzed events were acquired predominantly with triggers that provide real-time identification of electron and muon candidates. However, events satisfying any trigger requirement are considered.

This note documents a preliminary update to a previous search in the same final states [3, 4] that used up to 6.2 fb^{-1}, of which 1.1 fb^{-1} was collected during Run IIa, with the remaining data collected during Run IIb. In this update we discuss the reanalysis of the $\mu\mu$, ee , $\mu\mu_{\rm trk}$ and $ee_{\rm ICR}$ selections of the Run IIb data that now extends to an integrated luminosity of 7.5 fb^{-1}. The 1.1 fb^{-1} of Run IIa data are not reanalyzed, but are combined with this analysis to obtain the final results. This brings the total integrated luminosity for this result to 8.6 fb^{-1} for all channels.

II. EVENT SELECTION

The selection of signal-like events requires a primary $p\overline{p}$ interaction vertex (PV) that has at least three associated tracks, and is located within ± 60 cm of the center of the detector along the direction of the beam. Selected events must also contain a $Z \to \ell^+\ell^-$ candidate with a dilepton invariant mass $60 < m_{\ell\ell} < 150$ GeV.

The dimuon ($\mu\mu$) selection requires at least two muons identified in the outer muon system, matched to central tracks (combined muons) with transverse momenta $p_{\rm T} > 10$ GeV. Combined tracking and calorimeter isolation requirements are applied for both muons together, such that one muon does not have to be isolated if the other muon is sufficiently well isolated. Each muon track must satisfy $|\eta_{\rm det}| < 2$, where $\eta_{\rm det}$ is pseudorapidity measured with respect to the center of the detector. At least one muon must have $|\eta_{\rm det}| < 1.5$ and $p_{\rm T} > 15$ GeV. The distance of closest approach of each muon track to the PV in the plane transverse to the beam direction, d_{PV}, must be less than 0.04 cm for tracks with at least one hit in the silicon microstrip tracker (SMT). A track without any SMT hits must have $d_{PV} < 0.2$ cm, and its $p_{\rm T}$ is corrected through a constraint to the position of the PV. To reduce contamination from cosmic rays, the muon tracks must not be back-to-back in η and ϕ. The two muon tracks must also have opposite charge.

The $\mu\mu_{\rm trk}$ selection is designed to recover dimuon events in which one muon is not identified in the outer muon system. This selection requires exactly one muon identified in both the central tracking system and the outer muon system (referred to as a combined muon) with $|\eta_{\rm det}| < 1.6$ and $p_{\rm T} > 15$ GeV. To ensure that the $\mu\mu$ and $\mu\mu_{\rm trk}$ selections do not overlap, events containing any additional combined muons with $|\eta_{\rm det}| < 2$ and $p_{\rm T} > 10$ GeV are rejected. In addition, a central track with $|\eta_{\rm det}| < 2$ and $p_{\rm T} > 20$ GeV must be present. This track-only muon, which is associated with a muon that is only reconstructed in the central tracking system, is required to have at least one SMT hit and $d_{PV} < 0.02$ cm. It is also required to be isolated from other tracks and from calorimeter activity in an annulus surrounding the track vector. The combined muon and track-only muon must have opposite charges. For the very small fraction of events with more than one track meeting these requirements, the track whose invariant mass with the combined muon is closest to the Z boson mass (91.2 GeV) is chosen.

The dielectron (ee) selection requires at least two electrons with $p_{\rm T} > 15$ GeV that pass selection requirements based on the shapes of the electromagnetic showers in the calorimeter and separation of the showers from other depositions of energy. At least one electron must be identified in the central calorimeter (CC, $|\eta_{\rm det}| < 1.1$), and a second electron either in the CC or end calorimeter (EC, $1.5 < |\eta_{\rm det}| < 2.5$). The CC electrons must match central tracks or a pattern of hits consistent with a charged particle.

The $ee_{\rm ICR}$ selection requires exactly one electron in either the CC or EC with $p_{\rm T} > 15$ GeV, and an "ICR track" pointing toward the inter-cryostat region (ICR) of the calorimeter, $1.1 < |\eta_{\rm det}| < 1.5$, where the electromagnetic coverage is limited. The ICR track must be matched to a calorimeter energy deposit with $E_{\rm T} > 15$ GeV. When the electron is found in the EC, the ICR electron candidate is searched for in the nearest inter-cryostat region.

Jets are reconstructed in the calorimeter using the iterative midpoint cone algorithm [5] with a cone of radius 0.5 in the plane of rapidity and azimuth. The energy scale of jets is corrected for detector response, the presence of

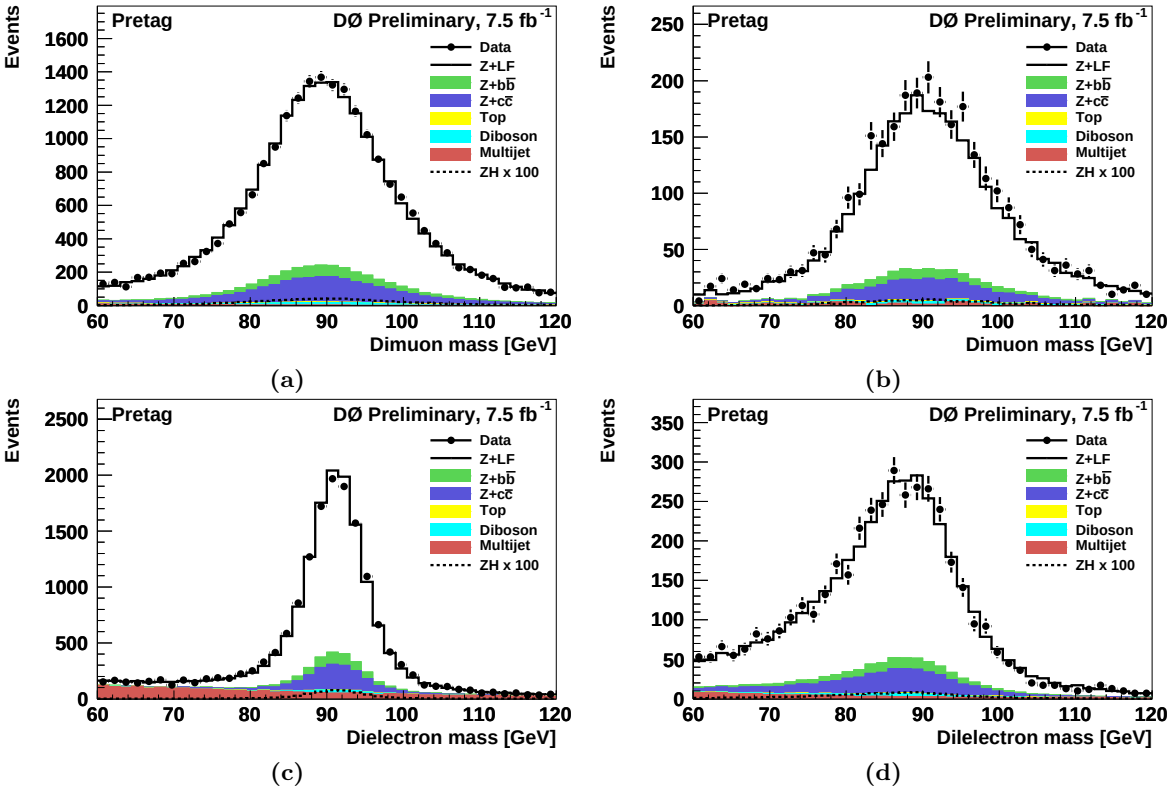

FIG. 1: The dilepton mass spectra in the (a) $\mu\mu$, (b) $\mu\mu_{\rm trk}$, (c) ee and (d) $ee_{\rm ICR}$ channels from the reanalyzed Run IIb dataset. Distributions are shown in the "pretag" control sample, in which all selection requirements except b-tagging are required. Signal distributions are scaled by factor of 100.

noise and multiple interactions, and energy deposited outside of the reconstructed jet cone. At least two jets with $|\eta_{\rm det}| < 2.5$ are required. We require one jet to have $p_{\rm T} > 20$ GeV and other jets to have $p_{\rm T} > 15$ GeV. For the ee and $ee_{\rm ICR}$ selections, jets that are matched to an electron by $\Delta\mathcal{R} = \sqrt{\Delta\eta^2 + \Delta\phi^2} < 0.5$ are removed from the event. In the $\mu\mu_{\rm trk}$ selection, the isolated track must be separated by $\Delta\mathcal{R} > 0.5$ from all jets. To reduce the impact from multiple interactions at high instantaneous luminosities, jets must contain at least two tracks matched to the PV. The dimuon and dielectron mass spectra, after requiring two leptons and two jets are shown in Fig. 1. The invariant mass of the dijet system (constructed from the two jets with the highest $p_{\rm T}$) in the combination of the all selections is shown in Fig 2.

To distinguish events containing a $H \to b\bar{b}$ decay, from background processes involving light quarks and gluons, jets are identified as likely to contain b-quarks (b-tagged) if they pass "loose" or "tight" requirements on the output of a boosted decision tree trained to separate b-jets from light jets. This discriminant is an improved version of the neural net b-tagging discriminant described in [6]. For $|\eta| < 1.1$ and $p_{\rm T} \approx 50$ GeV, the b-tagging efficiency for b-jets and the misidentification rate of light jets are, respectively, 72% and 6.7% for loose b-tags, and 47% and 0.4% for tight b-tags. Events with at least one tight and one loose b-tag are classified as double-tagged (DT). Events not in the DT sample that contain a single tight b-tag are classified as single-tagged (ST). The dijet $H \to b\bar{b}$ candidate is composed of the two highest $p_{\rm T}$ tagged jets in DT events, and the tagged jet plus the highest $p_{\rm T}$ non-tagged jet in ST events.

III. BACKGROUND ESTIMATION

The dominant background process is the production of a Z boson in association with jets, with the Z decaying to dileptons (Z+jets). The light-flavor component (Z+LF) includes jets from only light quarks (uds) or gluons. The heavy-flavor component (Z+HF) includes non-resonant $Z + b\bar{b}$ which has the same final state as the signal, and non-resonant $Z + c\bar{c}$ production. The remaining backgrounds are from $t\bar{t}$ and diboson production, and from multijet events in which jets are misidentified as leptons. We simulate ZH and inclusive diboson production with PYTHIA [7]. In the ZH samples, we consider the $\ell^+\ell^- b\bar{b}$, $\ell^+\ell^- c\bar{c}$, and $\ell^+\ell^-\tau^+\tau^-$ final states. The Z+jets and $t\bar{t} \to \ell^+\nu b\ell^-\bar{\nu}\bar{b}$

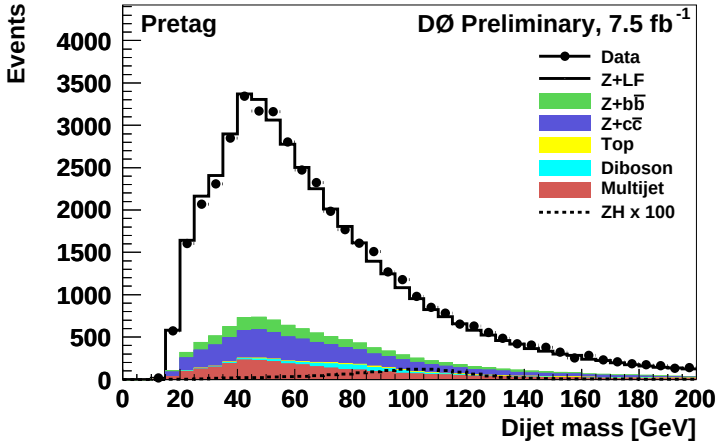

FIG. 2: Distribution in the pretag sample of the dijet invariant mass in the combined ee , $ee_{\rm ICR}$, $\mu\mu$ and $\mu\mu_{\rm trk}$ sample from the reanalyzed Run IIb dataset. The signal distribution is scaled by factor of 100.

processes are simulated with ALPGEN [8]. All simulated samples are generated using the CTEQ6L1 [9] leading-order parton distribution function (PDF).

The events generated with ALPGEN use PYTHIA for parton showering and hadronization. Because this procedure can generate additional jets, we use a matching procedure to avoid double counting partons produced by ALPGEN and those subsequently added by the showering in PYTHIA [8]. All samples are processed using a detector simulation program based on GEANT3 [10], and the same offline reconstruction algorithms used to process the data. Events from randomly chosen beam crossings are overlaid on the generated events to model the effect of multiple $p\overline{p}$ interactions and detector noise.

The cross section and branching ratio for signal are taken from Refs. [11, 12]. For the $t\bar{t}$ and diboson processes, the cross sections are taken from MCFM [14], which are calculated at next-to-leading order (NLO). The inclusive Z-boson cross section is scaled to next-to-NLO [15]. Additional NLO heavy-flavor corrections, calculated from MCFM, are applied to $Z + b\bar{b}$ and $Z + c\bar{c}$. To improve the modeling of the $p_{\rm T}$ distribution of the Z boson, the simulated Z boson events are reweighted to be consistent with the observed dielectron $p_{\rm T}$ spectrum in data [16].

The energies of simulated jets are modified to reproduce the resolution and energy scale observed in data. Scale factors are applied to account for differences in reconstruction efficiency between the data and simulation. Additional corrections are applied to improve agreement between data and background simulation, using a "pretag" control sample with negligible signal contribution that is obtained by applying all selection requirements except b-tagging. The $\mu\mu$, $\mu\mu_{\rm trk}$ and $ee_{\rm ICR}$ distributions are corrected for trigger efficiencies. For the ee channel, no correction is applied as the combination of all triggers is nearly 100% efficient. To improve upon the ALPGEN modeling of Z+jets, motivated by a comparison with the SHERPA generator [17], events are reweighted so that the pseudorapidities of the two jets with the highest $p_{\rm T}$ reproduce those distributions measured in the pretag data.

The multijet backgrounds are estimated from control samples in the data. For the $\mu\mu$ channel, the multijet control sample consists of events that fail the muon isolation requirements but otherwise pass the event selection. For the $\mu\mu_{\rm trk}$ channel, the combined muon and track must have same-sign charge. For the ee channel, the electrons must fail isolation and shower shape requirements. For the $ee_{\rm ICR}$ channel, the electron in the ICR must fail a requirement on the shape of the electromagnetic shower in the calorimeter.

The normalizations of the simulated and the multijet backgrounds are adjusted by scale factors determined from a fit to the $m_{\ell\ell}$ distributions in the inclusive and two-jet pretag data. This improves the accuracy of the background model and reduces the impact of systematic uncertainties that affect pretag event yields (e.g., uncertainties on luminosity and lepton identification). The region $40 < m_{\ell\ell} < 60$ GeV, where the multijet contribution is most prominent, is included in the fit to normalize the multijet sample to the actual multijet contribution. The inclusive sample constrains the lepton trigger and identification efficiencies, while the pretag sample, which includes jet requirements, is used to correct the Z+jets cross section by a common scale factor $k_{Z+\rm jets}$. The total event yields after applying all corrections and normalization factors are shown in Table I. The ST and DT signal yields for the individual channels are displayed in Table II.

	Data	Total Background	Multijet	Z+LF	Z+HF	Other	ZH
inclusive	1 369 260	1 360 988	125 154	1 198 533	34 176	1 999	20
pretag	45 730	45 339	2 930	34 543	6 965	900	14
ST	1 194	1 108	60	98	834	117	3.5
DT	452	428	16	6.3	283	123	3.9

TABLE I: Expected and observed event yields in the reanalyzed Run IIb dataset for all lepton channels combined after requiring two leptons (inclusive), after also requiring two jets (pretag), and after requiring at least one (ST) or two (DT) b-tags. The "Other" column includes diboson and $t\bar{t}$ event yields. The ZH sample yields are for $M_H = 115$ GeV.

Channel	ST	DT
ee	1.27	1.39
$ee_{\rm ICR}$	0.30	0.34
$\mu\mu$	1.69	1.91
$\mu\mu_{\rm trk}$	0.20	0.26

TABLE II: Signal yields in the ST and DT samples for each channel, assuming $M_H = 115$ GeV.

IV. MULTIVARIATE ANALYSIS

To exploit the kinematics of the $ZH \to \ell^+\ell^- b\bar{b}$ process, the energies of the candidate leptons and jets are adjusted within their experimental resolutions with a likelihood fit that constrains $m_{\ell\ell}$ to the mass and width of the Z, and the $p_{\rm T}$ of the $\ell^+\ell^- b\bar{b}$ system to the distribution expected for ZH events. Distributions of the dijet invariant mass spectra, before and after adjustment by the kinematic fit, may be seen in Fig. 3.

A multivariate analysis combines the most significant kinematic information into a single discriminant. Well-modeled kinematic variables are chosen as inputs for the analysis: the transverse momenta of the two b-jet candidates and the dijet mass, before and after the jet energies are adjusted by the kinematic fit; angular differences within and between the dijet and dilepton systems; the opening angle between the proton beam and the Z candidate in the rest frame of the Z boson [19]; and composite kinematic variables, such as the $p_{\rm T}$ of the dijet system and the scalar sum of the $p_{\rm T}$ values of the leptons and jets. A complete list of input variables is shown in Table III. For each assumed value of M_H a separate random forest (RF), consisting of 200 decision trees [18] is trained for ST and DT events. Each tree uses a randomly chosen subset of the simulated signal and background events. At each decision of each tree, a subset of ten of the twenty inputs is randomly chosen for consideration. The RF output is a performance-weighted average of the output from each decision tree. The RF outputs for the ee, $ee_{\rm ICR}$, $\mu\mu$ and $\mu\mu_{\rm trk}$ channels combined are shown separately for ST and DT events in Fig. 4.

	Multivariate Analysis Inputs
Jets:	m_{bb}, $p_{\rm T}^{bb}$, $p_{\rm T}^{b1}$, $p_{\rm T}^{b2}$, $\Delta\phi(b_1,b_2)$, $\Delta\eta(b_1,b_2)$
Post-fit jets:	m_{bb}, $p_{\rm T}^{b1}$, and $p_{\rm T}^{b2}$
Z candidate:	$p_{\rm T}^{Z}$, $\Delta\phi(\ell_1,\ell_2)$, $\Delta\eta(\ell_1,\ell_2)$, colinearity$(\ell_1,\ell_2)$
Z+jets:	$\Delta\phi(Z,bb)$
Topological:	$\cos\theta^*$, $m(\ell\ell bb)$, $H_T(\ell\ell bb)$, $m(\sum \vec{j}_i)$, $p_{\rm T}(\sum \vec{j}_i)$

TABLE III: Input variables to the multivariate analysis. Variables associated with the two b-jet candidates are the dijet-invariant mass m_{bb}; the transverse momenta of the dijet system $p_{\rm T}^{bb}$ and of the individual jets $p_{\rm T}^{b1}$ and $p_{\rm T}^{b2}$; and the angles $\Delta\phi(b_1,b_2)$ and $\Delta\eta(b_1,b_2)$ between the two jets. Variables associated with the Z candidate are the transverse momentum of the dilepton system $p_{\rm T}^{Z}$, the angles $\Delta\phi(\ell_1,\ell_2)$ and $\Delta\eta(\ell_1,\ell_2)$ between the dileptons, the cosine of the angle between the two leptons (colinearity) and the angle between the dilepton and dijet system $\Delta\phi(Z,bb)$. Topological variables are the cosine of the opening angle between the initial quark and the Z candidate in the $\ell\ell b\bar{b}$ rest frame $\cos\theta^*$; the invariant mass and total scalar energy sum of the $llbb$ system, $m(\ell\ell bb)$ and $H_T(\ell\ell bb)$; and the total invariant mass and transverse momentum of all jets in the event, $m(\sum \vec{j}_i)$ and $p_{\rm T}(\sum \vec{j}_i)$.

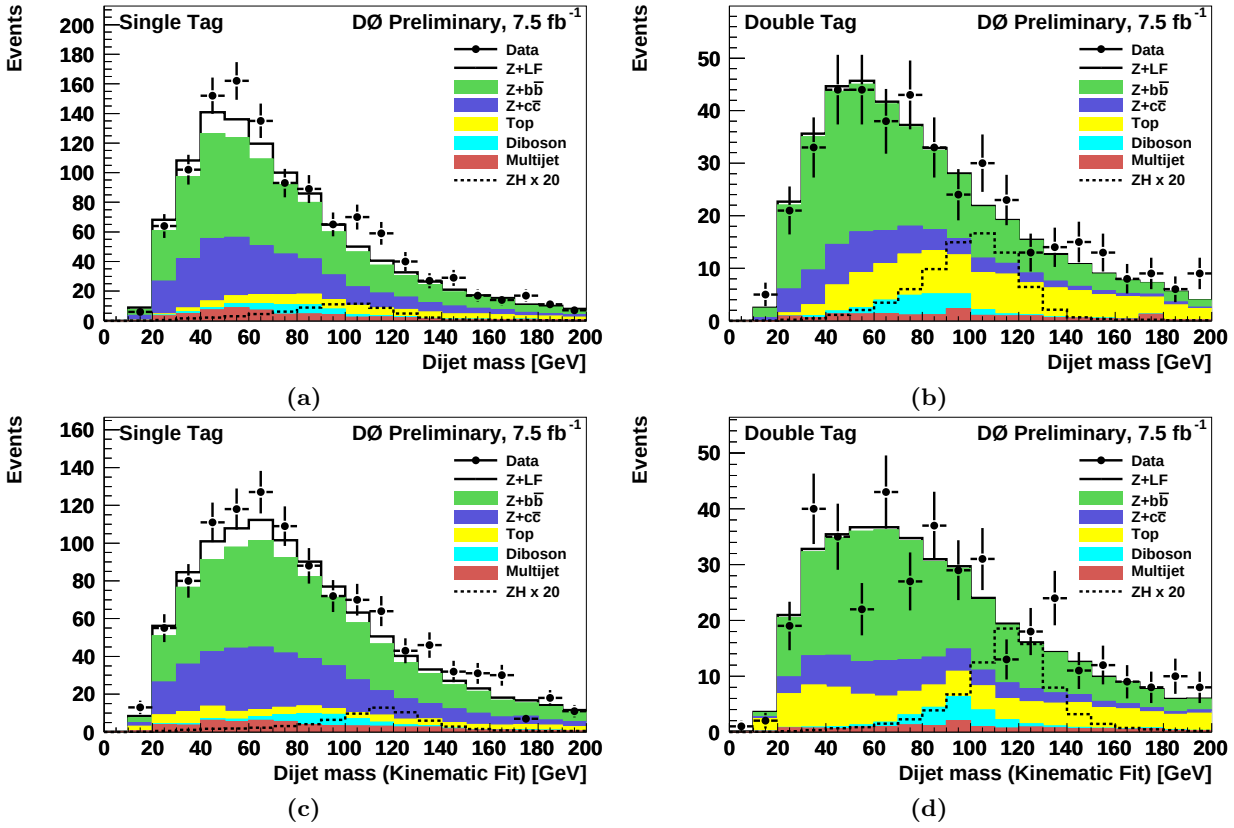

FIG. 3: Dijet invariant mass distributions before the kinematic fit in (a) ST events, and (b) DT events; and after the kinematic fit in (c) ST events and (d) DT events, combined for all lepton channels. Signal distributions are shown with the SM cross section multiplied by 20. The distributions are for the the reanalyzed Run IIb dataset.

V. SYSTEMATIC UNCERTAINTIES

Systematic uncertainties resulting from the background normalization are assessed for the multijet contribution (2–40%, depending on the channel), and from uncertainties on lepton efficiency effects (0.5-7%). The normalization of the Z+jets sample to match the pretag data constrains that sample to statistical uncertainty of the pretag data (<1%). However, the normalization of the $t\bar{t}$, diboson, and ZH samples acquires a sensitivity to the inclusive Z cross section, for which we assign an uncertainty of 8%. An additional systematic uncertainty (10%) for possible jet-dependent efficiency effects absorbed into $k_{Z+\mathrm{jets}}$ are applied to the $t\bar{t}$, diboson and ZH samples. The normalization to the pretag data, which is dominated by Z+LF, does not strongly constrain the cross sections of other processes. For Z+HF, a cross section uncertainty of 20% is determined from Ref. [14]. For other backgrounds, the uncertainties are 6%–10%. For the signal, the uncertainty is 6% [11]. The normalization procedure described in Section III reduces the impact of many of the remaining systematic uncertainties on the background size (except those related to b-tagging), but changes to the shape of the RF output distribution persist and are accounted for. Additional sources of systematic uncertainty include: jet energy scale, jet energy resolution, jet identification efficiency, b-tagging and trigger efficiencies, PDF uncertainties [13], data-determined corrections to the model for Z+jets, and modeling of the underlying event. The uncertainties from the factorization and renormalization scales in the simulation of Z+jets are estimated by scaling these parameters by factors of 0.5 and 2.

VI. RESULTS

We use the distributions in RF output for the ST and the DT samples in each channel and the corresponding systematic uncertainties to set limits. In addition to the reanalyzed 7.5 fb^{-1} Run IIb dataset, we also use the data from Run IIa which have not been re-analyzed. The total analyzed luminosity is thus 8.6 fb^{-1}. To take advantage of the sensitivity in the more discriminating channels, we provide separate distributions for each channel to the

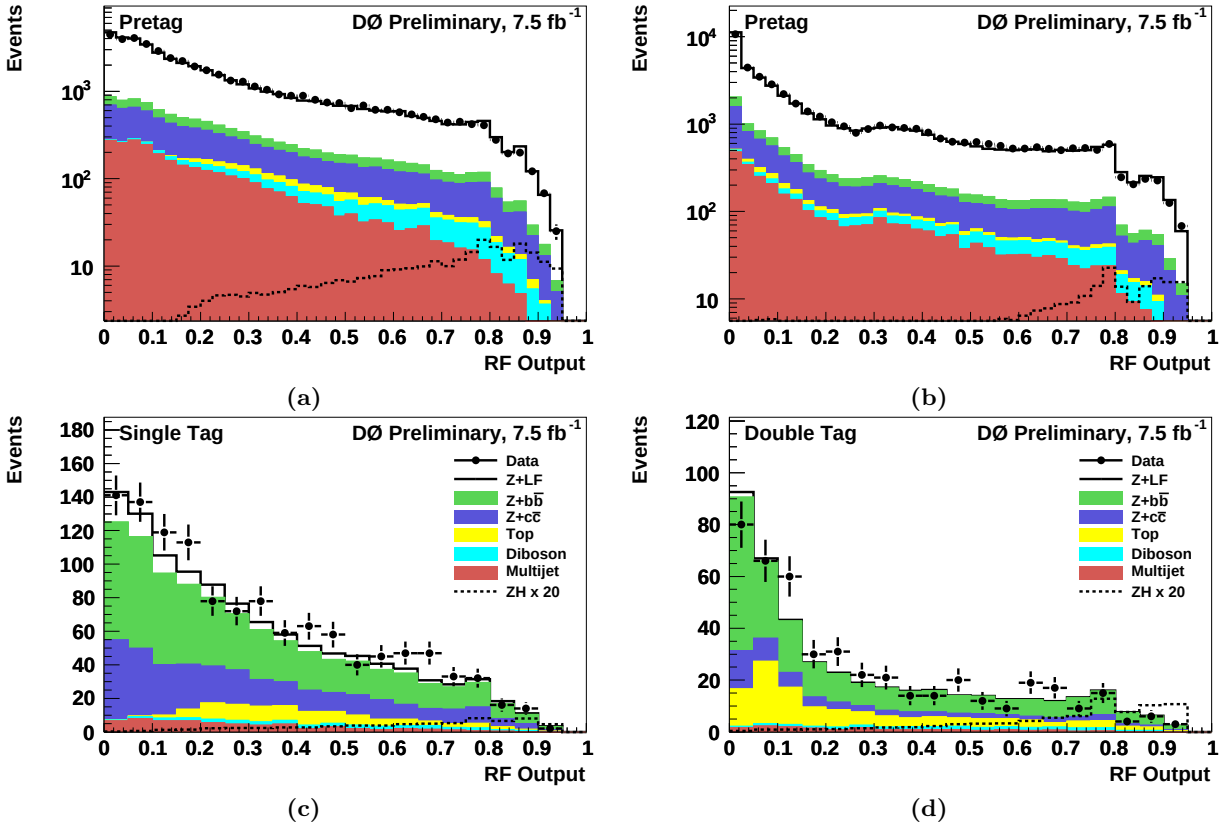

FIG. 4: RF output distributions for the ee , $ee_{\rm ICR}$, $\mu\mu$ and $\mu\mu_{\rm trk}$ channels combined assuming $M_H = 115\ GeV$ for (a) pretag events evaluated with the ST-trained RF, (b) pretag events evaluated with the DT-trained RF, (c) ST events evaluated with the ST-trained RF, (d) DT events evaluated with the DT-trained RF. Signal distributions are shown with the SM cross section multiplied by 20. The distributions are for the the reanalyzed Run IIb dataset.

limit-setting program.

We obtain 95% C.L. limits on the ZH cross section with a modified frequentist (CLs) method that uses a log likelihood ratio (LLR) of the signal+background hypothesis to the background-only hypothesis [20]. To minimize the effect of systematic uncertainties, the likelihoods of the B and S+B hypotheses are maximized by independent fits which vary nuisance parameters that model the systematic effects [21]. The correlations among systematic uncertainties are maintained across channels, backgrounds and signal, as appropriate. The post-fit background-subtracted RF distribution, combined for all channels, with the systematic uncertainty band resulting from the fitting procedure, is shown in Fig. 5.

Figure 6 shows the observed LLR for this Run IIb analysis added to the published Run IIa results [3], as a function of Higgs boson mass. Also shown are the expected (median) LLRs for the background-only and signal+background hypotheses, together with the one and two standard deviation bands about the background-only expectation. A signal-like excess would result in a negative excursion in the observed LLR. The upper limit on the cross section, expressed as a ratio to the SM cross section, as a function of M_H is presented in Table IV and Fig. 7. At $M_H = 115$ GeV, the observed (expected) limit on this ratio is 4.9 (4.8).

M_H (GeV)	100	105	110	115	120	125	130	135	140	145	150
Expected	3.4	3.7	4.2	4.8	5.3	6.5	8.4	11	14	22	34
Observed	2.5	2.6	3.1	4.9	6.4	8.9	9.9	15	25	34	50

TABLE IV: The expected and observed 95% C.L. upper limits on the SM Higgs boson production cross section for $ZH \to \ell^+\ell^- b\bar{b}$, expressed as a ratio to the SM cross section. Limits were obtained using the reanalyzed 7.5 fb^{-1} $\mu\mu$, $\mu\mu_{\rm trk}$, ee and $ee_{\rm ICR}$ Run IIb data discussed in this note, as well as the data from Run IIa that were not reanalyzed.

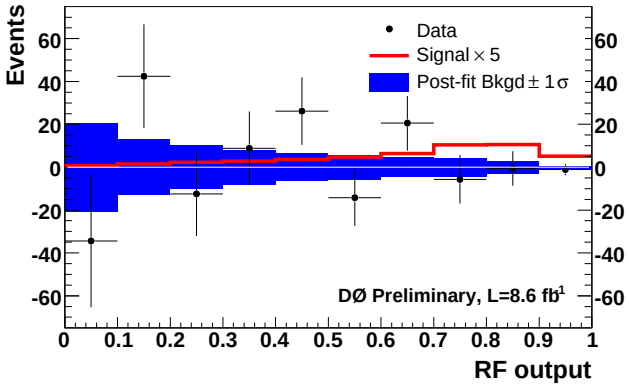

FIG. 5: Background subtracted RF distribution for M_H=115 GeV. Both ST and DT events are included. The dark blue region indicates the uncertainty after the fit to the background-only model. Results were obtained using the reanalyzed 7.5 fb^{-1} $\mu\mu$, $\mu\mu_{\rm trk}$, ee and $ee_{\rm ICR}$ Run IIb data discussed in this note, as well as the data from Run IIa that were not reanalyzed.

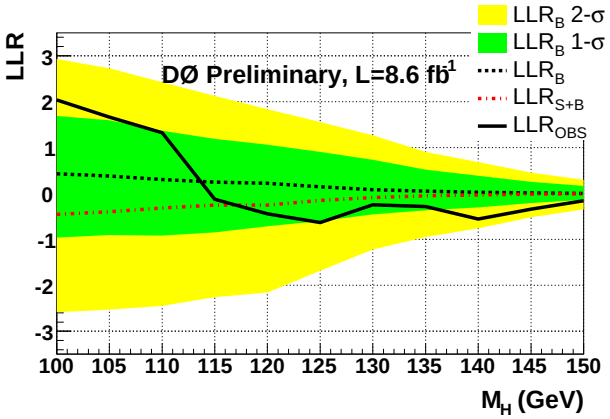

FIG. 6: Observed LLR as a function of Higgs boson mass. Also shown are the expected LLRs for the background-only (B) and signal+background (S+B) hypotheses, together with the one and two σ bands about the background-only expectation. Results were obtained using the reanalyzed 7.5 fb^{-1} $\mu\mu$, $\mu\mu_{\rm trk}$, ee and $ee_{\rm ICR}$ Run IIb data discussed in this note, as well as the data from Run IIa that were not reanalyzed.

Acknowledgments

We thank the staffs at Fermilab and collaborating institutions, and acknowledge support from the DOE and NSF (USA); CEA and CNRS/IN2P3 (France); FASI, Rosatom and RFBR (Russia); CNPq, FAPERJ, FAPESP and FUNDUNESP (Brazil); DAE and DST (India); Colciencias (Colombia); CONACyT (Mexico); KRF and KOSEF (Korea); CONICET and UBACyT (Argentina); FOM (The Netherlands); STFC and the Royal Society (United Kingdom); MSMT and GACR (Czech Republic); CRC Program and NSERC (Canada); BMBF and DFG (Germany); SFI (Ireland); The Swedish Research Council (Sweden); and CAS and CNSF (China).

[1] V.M. Abazov *et al.* (D0 Collaboration), DØ Note 6223-CONF (2011)
V.M. Abazov *et al.* (D0 Collaboration), Phys. Rev. Lett. **104**, 071801 (2010).
[2] V. M. Abazov *et al.* (D0 Collaboration), Nucl. Instrum. Methods Phys. Res. Sect. A **565**, 463 (2006);
[3] V.M. Abazov *et al.* (D0 Collaboration), Phys. Rev. Lett. **105**, 251801 (2010).

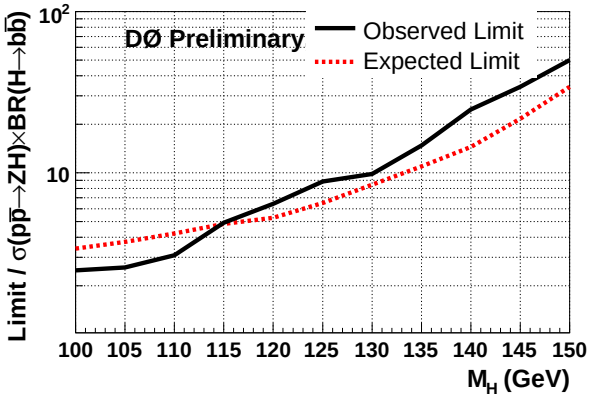

FIG. 7: Expected and observed 95% C.L. cross section upper limits compared to expected limit for the background-only hypothesis as a function of M_H. Limits were obtained using the reanalyzed 7.5 fb^{-1} $\mu\mu$, $\mu\mu_{\rm trk}$, ee and $ee_{\rm ICR}$ Run IIb data discussed in this note, as well as the data from Run IIa that were not reanalyzed.

[4] V.M. Abazov *et al.* (D0 Collaboration), DØ Note 6080-CONF (2010).
[5] G. C. Blazey et al., arXiv:hep-ex/0005012.
[6] V. M. Abazov *et al.* (D0 Collaboration), arXiv:1002.4224 [hep-ex]
[7] T. Sjöstrand *et al.*, Comput. Phys. Commun. **135**, 238 (2001). Version 6.409 was used.
[8] M. L. Mangano *et al.*, J. High Energy Phys. **0307**, 001 (2003). Version 2.11 was used
[9] J. Pumplin *et al.*, J. High Energy Phys. **07**, 012 (2002).
[10] R. Brun, F. Carminati, CERN Program Library Long Writeup W5013 (1993).
[11] J. Baglio and A. Djouadi, arXiv:1003.4266v2 [hep-ph].
[12] S. Dittmaier *et al.* [LHC Higgs Cross Section Working Group], arXiv:1101.0593v2 (2011).
[13] D. Stump *et al.*, J. High Energy Phys. **10**, 046 (2003).
[14] J. Campbell and R.K. Ellis, http://mcfm.fnal.gov/.
[15] R. Hamberg, W.L. van Neerven and W.B. Kilgore, Nucl. Phys. B**359**, 343 (1991), [*Erratum ibid.* B **644**, 403 (2002)].
[16] V. M. Abazov *et al.* (D0 Collaboration), Phys. Rev. Lett. **100**, 102002 (2008).
[17] T. Gleisberg *et al.*, J. High Energy Phys. 02 (2004) 056; J. Alwall *et al.*, Eur. Phys. J. C **53**, 473 (2008).
[18] A. Hoecker *et al.*, arXiv:physics/0703039v5 [physics.data-an].
[19] S. Parke and S. Veseli, Phys Rev D **60**, 093003 (1999).
[20] T. Junk, Nucl. Instrum. Methods Phys. Res., Sect. A **434**, 435 (1999); A. Read. J. Phys. G **28** 2693 (2002).
[21] W. Fisher, FERMILAB-TM-2386-E (2007).